Qiang Yu
Post-Doctoral Researcher
Department of Civil and Environmental
Engineering,
Northwestern University,
Evanston, IL 60208
e-mail: qiangyu@northwestern.edu

Zdeněk P. Bažant[1]
McCormick Institute Professor
W.P. Murphy Professor
Department of Civil and Materials Science,
Northwestern University,
Evanston, IL 60208
e-mail: z-bazant@northwestern.edu

John Bayldon
Post-Doctoral Researcher
e-mail: j-bayldon@northwestern.edu

Jia-Liang Le
Graduate Research Assistant
e-mail: jialiang-le@northwestern.edu

Department of Civil and Environmental
Engineering,
Northwestern University,
Evanston, IL 60208

Ferhun C. Caner[2]
Associate Professor of the Institute of Energy
Technologies,
Universitat Politècnica de Catalunya
e-mail: ferhun.caner@upc.edu

Wei Heok Ng
Post-Doctoral Researcher
e-mail: whn@umich.edu

Anthony M. Waas
Professor
e-mail: dcw@umich.edu

Department of Aerospace Engineering and
Mechanical Engineering,
University of Michigan,
Ann Arbor, MI 48109-2122

Isaac M. Daniel
W.P. Murphy Professor
Department of Civil Engineering and Mechanical
Engineering,
Northwestern University,
Evanston, IL 60208
e-mail: imdaniel@northwestern.edu

Scaling of Strength of Metal-Composite Joints—Part I: Experimental Investigation

Knowledge of the size effect on the strength of hybrid bimaterial joints of steel and fiber composites is important for new designs of large lightweight ships, large fuel-efficient aircrafts, and lightweight crashworthy automobiles. Three series of scaled geometrically similar specimens of symmetric double-lap joints with a rather broad size range (1:12) are manufactured. The specimens are tested to failure under tensile displacement-controlled loading, and at rates that ensure the peak load to be reached within approximately the same time. Two series, in which the laminate is fiberglass G-10/FR4, are tested at Northwestern University, and the third series, in which the laminate consists of NCT 301 carbon fibers, is tested at the University of Michigan. Except for the smallest specimens in test series I, all the specimens fail by propagation of interface fracture initiating at the bimaterial corner. All the specimens fail dynamically right after reaching the maximum load. This observation confirms high brittleness of the interface failure. Thus, it is not surprising that the experiments reveal a marked size effect, which leads to a 52% reduction in nominal interface shear strength. As far as the inevitable scatter permits it to see, the experimentally observed nominal strength values agree with the theoretical size effect derived in Part II of this study, where the size exponent of the theoretical large-size asymptotic power law is found to be −0.459 for series I and II, and −0.486 for series III. [DOI: 10.1115/1.3172254]

1 Introduction

Hybrid structures consisting of metals and fiber composites offer many advantages for the design of large lightweight ships [1] and fuel-efficient aircrafts. Metal-composite joints are a crucial element of such designs. Because of the cost of failure tests of large structures, laboratory tests must, in many situations, be conducted on a much reduced scale. Thus, it is essential to have a correct method to extrapolate the results obtained from small laboratory specimens to much larger structural parts.

For purely metallic structures, such extrapolation is relatively easy, since there is no deterministic size effect and the statistical size effect, which is relatively weak, is well understood. However, fiber composites are quasibrittle materials, which were shown [2–5] to exhibit, in general, a deterministic energetic size effect [6–10]. This size effect is much stronger than the statistical size effect observed in fatigue-embrittled metals.
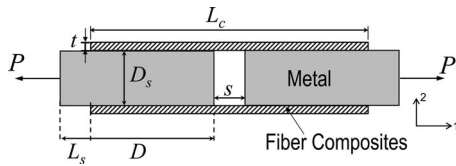
Fig. 1 Geometry of double-lap hybrid joint

In fracture mechanics of bimaterial joints, significant advances have already been made [11–16]. The same can be said of adhesive layers between two dissimilar materials [17–20]. However, the scaling of the strength of these joints does not seem to have been studied.

One complication in fracture mechanics of these joints is that the singularity exponent of the stress field at the tip of an interface crack is a complex number. In linear elastic fracture mechanics (LEFM), a nonzero imaginary part implies an oscillating crack opening profile with interpenetration of the opposite crack faces. After protracted debates, two conclusions eventually emerged [21,22]: First, the distance from crack tip over which LEFM predicts interpenetrations to occur is generally much smaller than the size of the fracture process zone (FPZ), which means that the interpenetrations are outside the range of validity of the LEFM solution. Second, in spite of the interpenetrations, the complex singularity field does give the correct energy release rate of a propagating interface crack [17,23,24], which is what really matters.

Another complication in hybrid joints is that the fracture initiates from the stress singularity at a reentrant corner. The same complication, of course, occurs for reentrant corners in homogeneous materials. For a finite corner angle, the real part of the exponent of the corner tip stress singularity in bimaterial, as well as homogeneous situations, is larger than $-\frac{1}{2}$. This implies the energy release rate at the corner to vanish, and so it is impossible to satisfy the energy balance for a sharp (LEFM) crack initiating from the corner. The way around this problem is to recognize that a finite FPZ must form at the corner first.

One way to approximate such an FPZ is to postulate an equivalent LEFM crack at the corner [25,26]. Together with the crack tip singularity, this introduces a pair of stress field singularities located very close to each other. But then a rigorous LEFM analysis becomes difficult and messy.

A better and more physical approach is to admit at the outset that both singularities actually lie within the domain of one FPZ, which envelops both the corner and crack tip. A realistic approximate way to deal with it is to consider that a cohesive crack with a given softening stress-separation relation emanates from the corner. Combining the exact corner and crack tip singular fields with the finite element analysis of cohesive fracture, Bažant and Yu [27] presented an accurate solution of this problem for symmetrically loaded corners of various angles in a homogeneous material, and derived by means of asymptotic matching the law of size effect in fracture at such corners [27]. However, for reentrant corners in bimaterial joints, the size effect appears to be unknown. To determine it is the goal of this two-part study.

The first part of this study presents experimental evidence of the size effect in hybrid joints. The second part, which follows, deals with the analytical formulation of the size effect, based on bimaterial interface fracture mechanics. Computational simulation of the size effect in hybrid joints is planned for a subsequent paper.

2 Choice of Test Specimens

Two types of specimen geometry and composition have been investigated—one at Northwestern University and another at the University of Michigan. The geometry of the double-lap metal-composite joints tested is shown in Fig. 1.

In each hybrid joint, there are eight bimaterial corners: four interior and four exterior. Based on the singularity exponent, the interface crack should start at the interior ones. The test results confirm it.

The nominal strength σ_N is a load parameter with the dimension of stress, and is here defined as $\sigma_N = P_{max}/bD$. Here, P_{max} is the maximum load (which must be the failure load if load control is used), b is the width of the joint (in the third dimension), and D is the characteristic size (or dimension) of the joint (any in-plane dimension can be chosen as D since only the relative sizes matter). For this study, D is the length of the interface.

2.1 Specimen Dimensions. The greater the size effect ratio compared with the width of the scatter band, the lower is the ambiguity in identifying the size effect. For the typical random scatter in the testing of fiber composites, it is found that the size range must be at least 1:8 to produce a sufficient size effect range, and thus achieve unambiguous test results with a small enough error [8,28,10].

To avoid manufacturing specimens of variable sizes, which is normally more costly, some researchers tried to exploit the LEFM energy release rate function $g(\alpha)$ to deduce the size effect indirectly from specimens of one maximum cross section dimension, but different in shape or different in notch depth. Unfortunately, this method is fraught by large statistical error because the range of the so-called brittleness number [8,10] achievable by varying the geometry at constant maximum size is too limited [29].
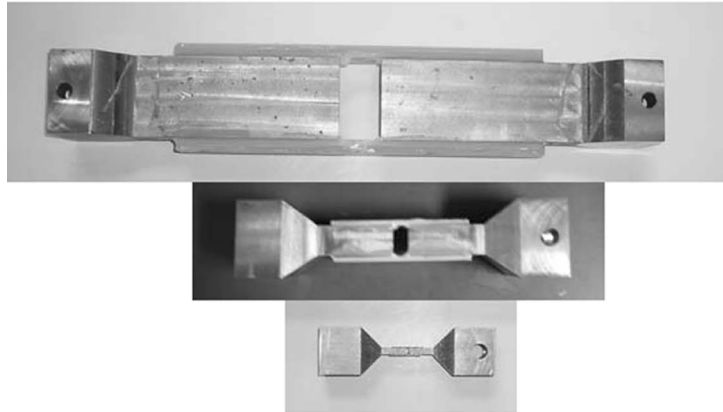
Two series of geometrically similar specimens using the same type of laminate were manufactured and tested at Northwestern University (see Figs. 2(a) and 2(b)). A third series with a slightly different geometry was manufactured and tested at the University of Michigan to explore the size effect for a different type of laminate (see Fig. 2(c)).

In the first two test series, the steel blocks at each end are enlarged to accommodate the connectors of the steel chain through which the tensile load is applied. For the third test series, an additional 38.1 mm length is added to the steel bars at both ends so that wedge grips can be used for loading. Except for the aforementioned support parts, all the specimens within each test series are geometrically similar (which means the dimensions of D, D_s, L_c, L_s, t, and s have the same ratios for all the sizes). Such scaling makes detection and calibration of the size effect particularly easy because the material failure criteria expressed solely in terms of stresses and strains predict no size effect, i.e., the same with the nominal strength σ_N, regardless of the specimen size [6–9].
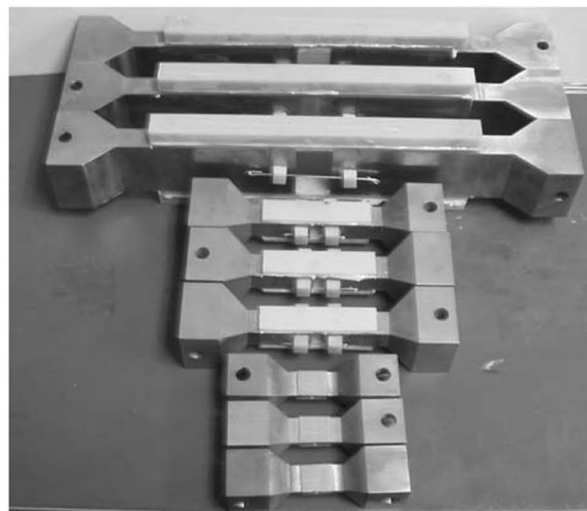
The specimens of series I and II were loaded in tension through chains at both ends to ensure that the tension resultant is centric. However, the specimens of series III were fixed at both ends against rotation and loaded at both ends by wedge grips. In general, such end fixtures could lead to tensile force eccentricity. However, thanks to careful attention to the alignment of end supports, the strain gauges on the opposite sides of the specimen gave nearly identical readings. This confirms that the resultant was centric.

The size ratios have been selected as 1:4:12 for series I and II, and 1:3:9:12 for test series III, both of which suffice to meet the aforementioned required breadth of the size range. There are three specimens in series I, and nine specimens in each of series II and III. In test series I there is thus only one specimen for each characteristic size D. In test series II there are three for each size, and in series III there are three for the two larger sizes, two for the smaller size, and one for the smallest size. The specimen dimensions in all the series are listed in Table 1. In series I, the smallest specimen was found to fail by tensile fracture of the laminate rather than by shear fracture along the interface, and to avoid it,
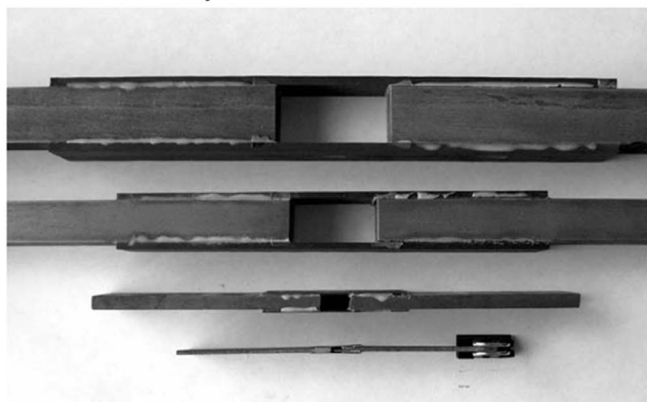
Fig. 2   Specimens of (*a*) test series I, (*b*) test series II, and (*c*) test series III

the relative laminate thickness in series II has been doubled. The other dimensions for series I and II are the same; the width b = 20 mm in series I and II, and b = 25.4 mm in series III. The optimal selection of D_s, s, L_c, and L_s was determined by finite element simulation [30] in order to ensure that: (1) the singular stress fields introduced by bimaterial corners would not appreciably interfere with each other, and that (2) the steel block would still be in the elastic range when the hybrid joint fails.

Table 1   Dimensions of specimens

Specimen	s (mm)	L_s (mm)	L_c (mm)	D_s (mm)	t (mm)	D (mm)
I-S-1	2.5	2.5	22.5	5	0.794	10
I-M-1	10	10	90	20	3.175	40
I-L-1	30	30	270	60	9.525	120
II-S-1,2,3	2.5	2.5	22.5	5	1.588	10
II-M-1,2,3	10	10	90	20	6.35	40
II-L-1,2,3	30	30	270	60	19.05	120
III-SS-1	3.175	6.35	15.875	1.5875	0.2413	6.35
III-S-1,2	9.525	19.05	47.625	4.7625	0.7366	19.05
III-M-1,2,3	28.575	57.15	142.875	14.2875	2.1844	57.15
III-L-1,2,3	38.1	76.2	190.5	19.05	2.9718	76.2

I: test series I; II: test series II; III: test series III.

2.2 Properties of Composites. The metal and the laminate are the same for series I and II. The metallic part is made of 1018 cold rolled steel having elastic modulus $E=200$ GPa and Poisson's ratio $\nu=0.3$. The composites of the hybrid joint are fiberglass-epoxy laminates (G-10/FR4 Epoxy Grade procured from McMaster-Carr, Inc.). The G-10/FR4 Garolite, manufactured by continuous weaving, is a glass-cloth laminate with epoxy resin binder. Although excellent tensile strength and high impact resistance is expected for the G-10/FR4 Garolite, the supplier does not provide precise information about its material properties, which are essential for theoretical analysis and numerical simulation. To determine these properties for series I and II, three types of test are carried out.

(1) The uniaxial tensile test is used to obtain the in-plane Young's modulus E_{11} and Poisson's ratio ν_{13}. Among different standard tensile test methods for composite materials, the Composites Research Advisory Group (GRAG) method 302, used to test axially orthotropic woven fiber-reinforced laminates [31], is selected. Accordingly, three specimens of length $L=260$ mm, width $W=20$ mm, thickness $t=1.588$ mm, and tab length $L_t=50$ mm are cut from one and the same G-10/FR4 Garolite sheet (see Fig. 3). To measure the longitudinal and transverse strains, a strain gauge is glued at the center to each specimen.

(2) The uniaxial compressive test is used to obtain the through-thickness Young's modulus E_{22} and Poisson's ratio ν_{21}. In contrast to the in-plane elastic properties and transverse shear modulus G_{12}, there exists no recognized national or international standard for measuring E_{22} and ν_{21}. The reason seems to be partly that strain and stress gradients are introduced by fabrication of thick sections [32], and partly

that the through-thickness properties are dominated by the polymer matrix, which is isotropic. For the compressive test, three laminate prisms, with dimensions of $35 \times 15 \times 15$ mm^3, are cut from the same G-10/FR4 Garolite block and then bonded to a $50 \times 35 \times 35$ mm^3 steel block at each end (see Fig. 3). The strains of two gauges, glued at the opposite sides of each specimen, are averaged to eliminate a possible effect of compression eccentricity.

(3) The Iosipescu V-notched beam test is used to obtain the through-thickness shear modulus G_{21}. Three flat rectangular specimens with dimensions $76 \times 19.05 \times 4$ mm^3 are made, and two 90 deg angle notches, with faces oriented at ± 45 deg to the longitudinal axis, are cut to the depth of 3.81 mm at the center of both edges (see Fig. 3). Biaxial strain gauges are bonded between the notches to measure the shear strains.

The following in-plane and through-thickness material properties of G-10/FR4 Garolite are obtained: $E_{11}=30.0$ GPa, $\nu_{13}=0.17$, $E_{22}=9.5$ GPa, $\nu_{21}=0.20$, and $G_{12}=3.0$ GPa.

The adhesive, which glues the steel and G-10/FR4 Garolite together, is the E-60HP metal-plastic bonder procured from McMaster-Carr, Inc. Although E-60HP provides high shear strength and peel resistance, its strength varies widely with the surface treatment. In test series I, the steel surface is sandblasted by extra coarse aggregate with glass beads (procured from Potters Industries, Inc.). In test series II, the steel surface is smooth.

In series III, the metallic part is the same as in series I and II. The composites are made using Newport NCT301 carbon laminates, which is a unidirectional tape laminate with an epoxy resin matrix, and the adhesive is NB1101 0.030 psf epoxy film adhe-
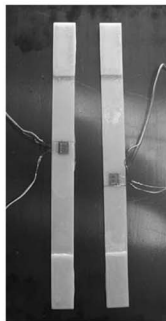
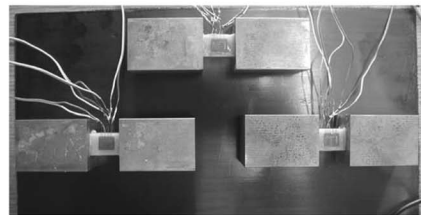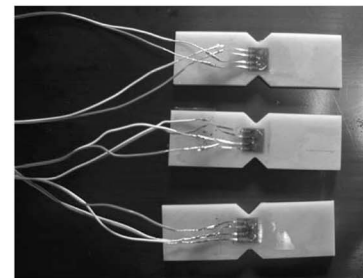## Uni-axial tension   Uni-axial compression   V-notch shear

(a)   (b)   (c)

Fig. 3   Tests giving basic material properties of laminates: (*a*) tensile test, (*b*) through-thickness compressive test, and (*c*) V-notched beam test
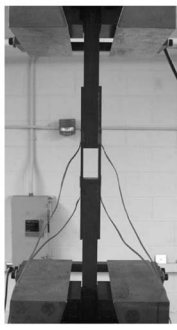
Fig. 4 (*a*) **Test setup at Northwestern University;** (*b*) **test setup at the University of Michigan**

sive. Both laminates and adhesives are produced by Newport Adhesives and Composites, Inc. According to the material data sheet, the properties for the uniaxial composites are: $E_{11}=125.5$ GPa, $\nu_{12}=\nu_{31}=0.304$, $E_{22}=9.0$ GPa, and $G_{12}=5.6$ GPa.

3 Size Effect Test

All the specimens are loaded under displacement control by a Material Testing Systems, Inc. (MTS) servohydraulic testing system. To ensure centric tensile load, a steel chain is connected to the specimen by a cylindrical pin for series I and II; see Fig. 4(*a*).

In test series III, the specimens are fixed at both ends by wedge grips (Fig. 4(*b*)).

To isolate the rate dependence from the size effect, the fracture process zone in specimens of different sizes should get fully developed within about the same time [28]. To meet this requirement, the loading rates (rates of the stroke of loading piston) are chosen as 0.09 mm/min, 0.3 mm/min, and 0.9 mm/min for different sizes in test series I. At these rates, the peak loads are reached within 7–10 min. In test series II, the loading rates were 0.2 mm/min, 0.5 mm/min, and 0.8 mm/min, and the peak loads were reached within 5–6 min for all the sizes. In test series III, the loading rates were 0.152 mm/min, 0.456 mm/min, 0.760 mm/min, and 1.216 mm/min, and it took 3–6 min for all the specimens to reach their peak loads. Unlike test series I, in which only the load and stroke data were recorded, two linear variable displacement transducer (LVDT) devices in series II (Fig. 4(*a*)) and four strain gauges in series III (Fig. 4(*b*)) are installed at the opposite sides of each specimen to measure the relative displacement or strains and monitor a possible load eccentricity.

All the specimens failed in a brittle manner, which is documented by a sudden load drop after the specimens reached their peak loads in the load-displacement plots (see Figs. 5(*a*)–5(*c*)). The failure was dynamic and it occurred right after the peak load had been reached, and in the largest specimens there was a loud boom. All the specimens plotted in Figs. 5(*b*) and 5(*c*) exhibited interfacial failure.

Beside the interfacial failure in medium and large size specimens, another type of failure occurred in test series I. As shown in Fig. 5(*d*), the laminates of the smallest specimen failed by tensile fracture across the laminate, and a crack along the metal-
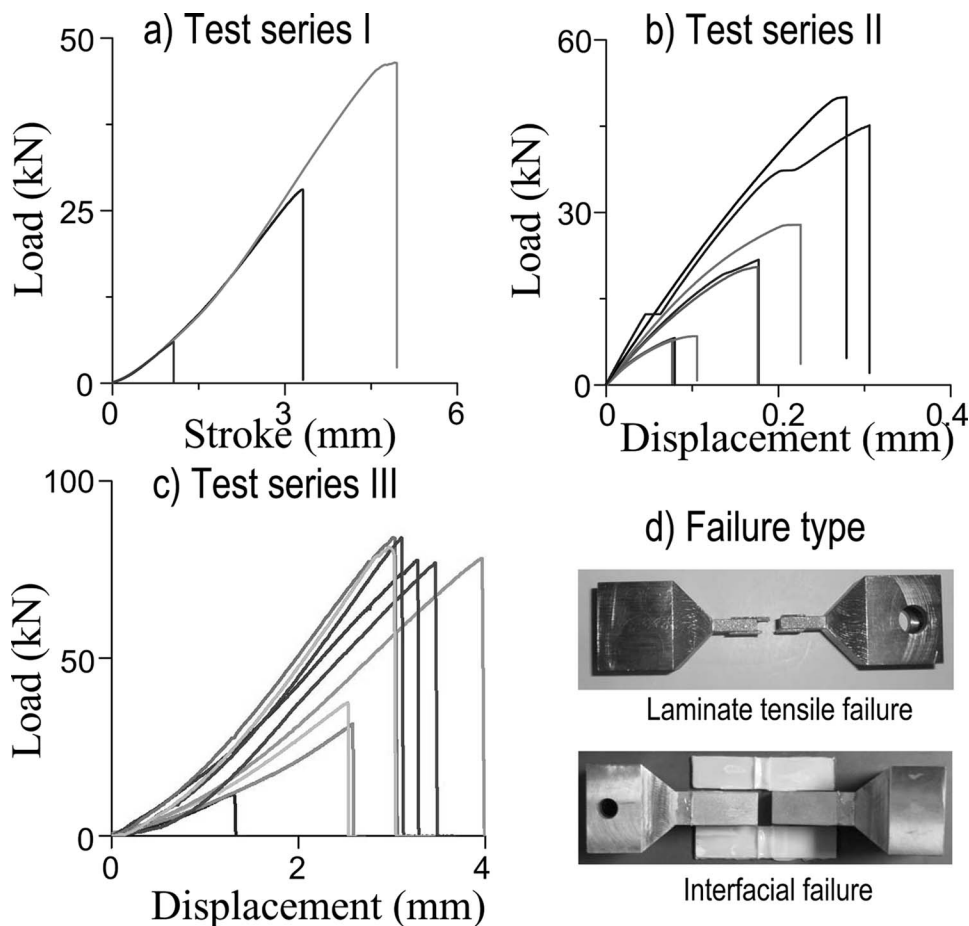

Fig. 5 **Load-displacement deformation curves** (*a*) **of test series I,** (*b*) **of test series II,** (*c*) **of test series III, and** (*d*) **tensile fracture in laminates and shear fracture in bimaterial interface**

Table 2 Recorded peak load

Specimen	P (kN)	Specimen	P (kN)	Specimen	P (kN)	Specimen	P (kN)
I-S-1	6.00[a]	I-M-1	28.09	I-L-1	46.49		
II-S-1	8.19	II-M-1	21.85	II-L-1	–		
II-S-2	7.89	II-M-2	27.90	II-L-2	50.01		
II-S-3	8.51	II-M-3	20.57	II-L-3	45.40		
III-SS-1	11.60	III-S-1	31.51	III-M-1	76.81	III-L-1	83.66
–	–	III-S-2	37.48	III-M-2	78.01	III-L-2	83.87
–	–	–	–	III-M-3	78.77	III-L-3	81.27

[a]Failed by tensile fracture of laminate.

composite interface could not develop fully. Therefore, the failure data for the smallest specimens are not comparable, and only the data for the medium and largest specimens of series I can be used. Obviously, the laminate thickness was too small in relation to the interface length, and it was for this reason that the laminate thickness was doubled for series II. Tensile fracture of the laminate also occurred in several of the smaller specimens in test series III. To identify the size effect exclusively on the interface shear strength, these tests had to be ignored.

4 Interpretation of Experimental Results

As known from the theory of crack interactions and stability [33], the fractures propagate from all the four inner corners simultaneously in a stable manner while the load is increasing (except for small differences due to inevitable random deviations from perfect symmetry). After the peak load, only one of the four interface cracks can grow, while the others must unload. The observations from the tests support this kind of fracture evolution.

The recorded peak loads for all the specimens of series I, II, and III are listed in Table 2 (only two peak loads are listed for the largest specimens of series II, because the electronic equipment malfunctioned in one test). The corresponding plots of log σ_N versus log D, as shown in Figs. 6 and 7, for all test series, display a conspicuous size effect. For a fourfold size increase, the nominal strength reduction is significant (52% in series II and 40% in series III). In series I, the σ_N value for the smallest specimen, shown by a solid circle, cannot be used to calibrate the size effect law because the failure occurred in the laminate rather than the interface. Nevertheless, the σ_N value that would correspond to the interface failure must be higher than the solid circle point, and thus, series I, too, confirms a strong size effect.

The test data may be fitted by the size effect equation

$$\sigma_N = \sigma_0 (1 + D/D_0)^\lambda \qquad (1)$$

which is derived by asymptotic matching from fracture mechanics in Part II of this study; σ_0, D_0, and λ are constants. D_0 is called the transitional size, which generally equals the material charac-

teristic length [8,10] times a geometry dependent factor obtainable from the equivalent LEFM. Since the size range is not broad enough and the scatter is not small enough to determine the exponent λ purely experimentally, the values $\lambda = -0.459$ for series I and II, and $\lambda = -0.486$ for series III, which give the asymptotic slopes in logarithmic size effect plots, are derived theoretically in Part II of this study [34]. They are seen to agree with the present test data.

Using nonlinear statistical regression of the test data, one finds $\sigma_0 = 47.8$ MPa and $D_0 = 20.77$ mm for test series II, with $\omega = 8.7\%$, and $\sigma_0 = 98.0$ MPa and $D_0 = 18.75$ mm with $\omega = 10.5\%$ for series III (where ω is the coefficient of variation of the regression errors, i.e., the standard error of regression divided by the data mean). When plotted in the double-logarithmic scales (Figs. 6 and 7), the negative curvature documenting the transition from quasiplastic behavior at small sizes to the LEFM for large sizes is clearly apparent. For test series I, the data exist for only two sizes, which is not statistically sufficient to fit a formula with two free parameters. However, the large-size asymptote of slope -0.459 agrees with series I data (see Fig. 6).

Figure 5(b) shows the load-displacement curves of series II specimens, all of which failed due to fracture propagation in the bimaterial interface. Note the sudden dynamic load drop after the peak for all the sizes. This means that the post-peak equilibrium path exhibits a snapback (i.e., runs to the left of the load drop). For all quasibrittle materials, the snapback takes place when the large-size asymptote is approached closely enough. In the fracture testing of concrete, the size above which the snapback occurs is quite large. The fact that here the snapback occurs even for the smallest specimen available means that, compared with other quasibrittle materials such as concrete, the stress-separation diagram of the cohesive interface crack must have a relatively steeper de-
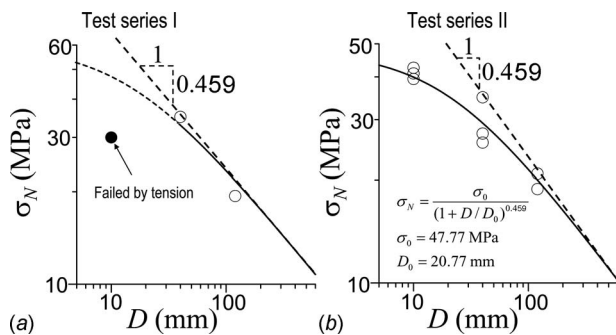

Fig. 6 Measured nominal strength values compared with optimum fit by size effect formula (solid curve): (a) test series I and (b) test series II
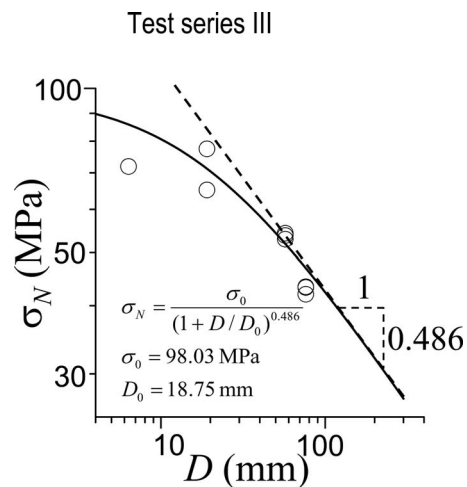

Fig. 7 Measured nominal strength of test series III compared with optimum fit by size effect formula
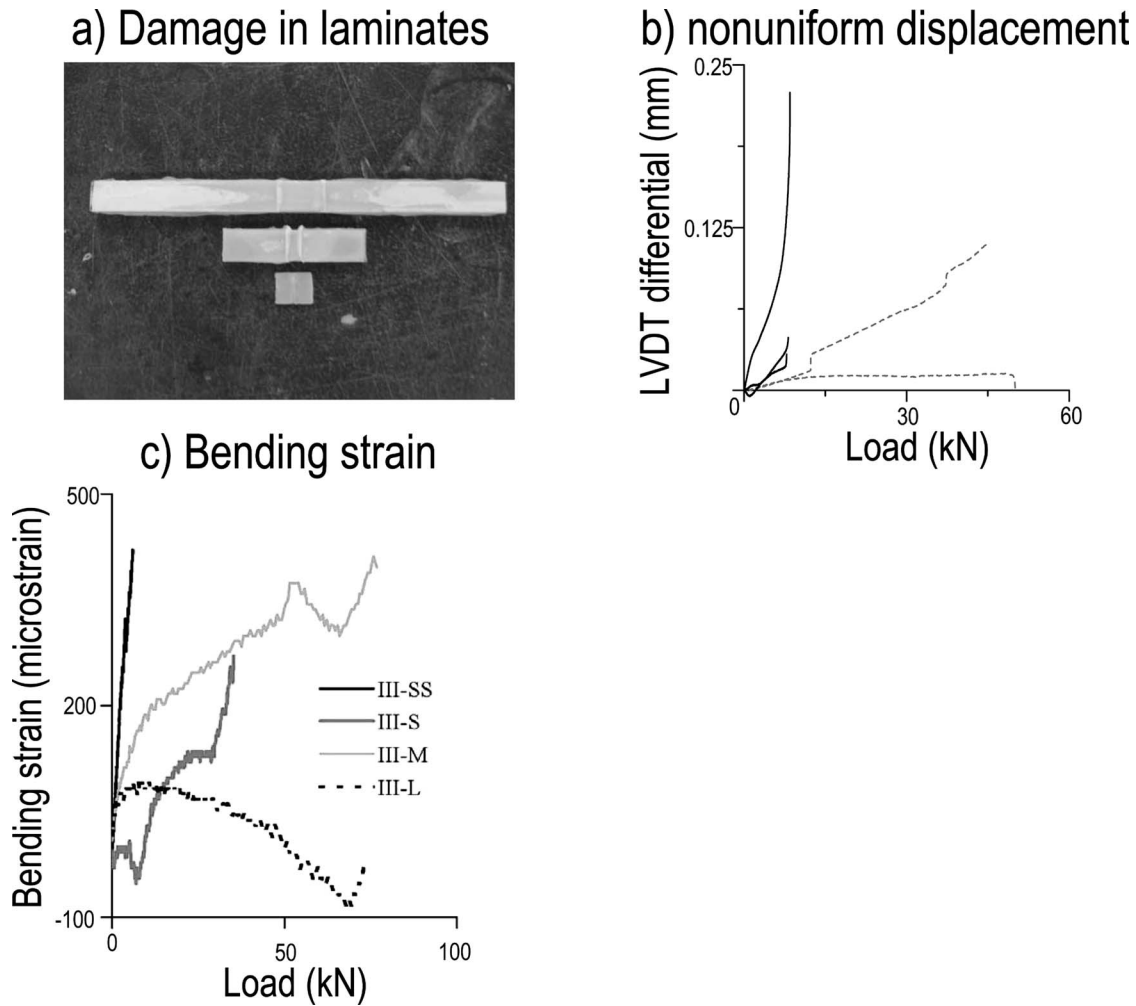
a) Damage in laminates

b) nonuniform displacement

c) Bending strain

Fig. 8 (*a*) Delamination pattern observed in test series II, (*b*) differences in readings of opposite LVDT gauges in test series II, and (*c*) strain differences at opposite specimen sides recorded in test series III

scent, and the FPZ must be narrower [8,28] (a similar conclusion for fracture within laminates is also obtained in a previous study [35]).

Before the peak load, the FPZ must grow simultaneously at all the corners. But after the peak, the interface crack propagates from one corner only. From which one? This is decided by the corner singularity exponents. In the analytical study [34], which follows in Part II of this study, the stress singularity at the inner bimaterial corners (the corners closer to the center of test specimen) is much stronger than that at the outer corners. Thus, the crack should propagate from one of the four inner corners, or generally from a corner at which the stiffer bar (in this case the steel bar) terminates. This is confirmed by studying the damage pattern of the laminates after the failure test (see Fig. 8(*a*)). The formation of the cohesive interface fracture can be inferred from the delamination marks, which form because the crack advances in jumps. In the laminates of the small- and medium-size specimens of series II, the delamination marks are seen only in the region near the interior corners, while at the exterior corners, the laminates are almost intact. The crack development in the bimaterial interface is further documented by the laminate damage pattern in the large specimens of series II (see the photo in Fig. 8(*a*)), which shows the delamination to start from the inner corner and then gradually grows through the whole interface. A similar evolution of the delamination is also observed in series III.

For perfectly centric axial tensile loading, no bending moment will develop until the fracture localizes into one of the four interfaces in the hybrid joint. This means that the LVDT or strain gauges on opposite sides should give similar readings. The readings were not identical, but their difference was small enough to be attributed to inevitable errors in the alignment and material fabrication.

Figure 8(*b*) shows, by solid and dashed lines, the evolution of displacement differential with increasing load. Note that the small displacement nonuniformity in the small-size specimens has almost no effect on the peak load. For the two large-size specimens, one specimen displays a negligible displacement difference (a long horizontal portion of the dashed line), and the other shows substantial nonuniform displacement (ascending dashed line). Nonetheless, the peak load difference between these two specimens is insignificant compared with the coefficient of variation in the nonlinear size effect regression, which is $\omega=8.7\%$.

Unlike series I and II, the specimens of series III are loaded by wedge grips at both ends. This is a support condition which might introduce axial load eccentricity, with asymmetric stresses in the opposite laminates. Nevertheless, according to the readings of the four strain gauges bonded to the opposite sides of specimens, the difference between the strains at opposite sides was negligible,

with no appreciable effect on the nominal strength (see Fig. 8(*c*), which shows the typical strains due to bending moment for all the sizes).

5 Conclusions

The strength of metal-composite hybrid joints exhibits a strong size effect. A fourfold increase in size may cause the nominal strength to drop by more than 50%.

Experiments on geometrically similar specimens of different sizes agree with the theoretical size effect law [34], representing a smooth transition from quasiplastic behavior in the theoretical small-size limit to brittle (LEFM) behavior in the large-size limit.

Observation of the damage patterns in the failed specimens supports the theoretical prediction that the interface fracture should initiate at the corner, at which the stiffer of the two joined bars terminates.

The documented presence of size effect implies that the strength of metal-composite hybrid joints cannot be calculated from material models with failure criteria expressed solely in terms of stress and strain, which have been typical of elastic, plastic, and plastic-damage models. Rather, cohesive fracture mechanics or nonlocal damage mechanics, in which the failure criterion involves some type of energy or material length, must be used. Otherwise, the strength of large hybrid joints would be dangerously overestimated.

Acknowledgment

References

[1] Barsoum, R. S., 2003, "The Best of Both Worlds: Hybrid Ship Hulls Use Composites & Steel," The AMPTIAC Quarterly, **7**(3), pp. 55–61.
[2] Bažant, Z. P., Daniel, I. M., and Li, Z., 1996, "Size Effect and Fracture Characteristics of Composite Laminates," ASME J. Eng. Mater. Technol., **118**(3), pp. 317–324.
[3] Bažant, Z. P., Kim, J.-J. H., Daniel, I. M., Becq-Giraudon, E., and Zi, G., 1999, "Size Effect on Compression Strength of Fiber Composites Failing by Kink Band Propagation," Int. J. Fract., **95**, pp. 103–141.
[4] Bažant, Z. P., Zhou, Y., Daniel, I. M., Caner, F. C., and Yu, Q., 2006, "Size Effect on Strength of Laminate-Foam Sandwich Plates," ASME J. Eng. Mater. Technol., **128**(3), pp. 366–374.
[5] Bažant, Z. P., Zhou, Y., Novák, D., and Daniel, I. M., 2004, "Size Effect on Flexural Strength of Fiber-Composite Laminate," ASME J. Eng. Mater. Technol., **126**, pp. 29–37.
[6] Bažant, Z. P., 1984, "Size Effect in Blunt Fracture: Concrete, Rock, Metal," J. Eng. Mech., **110**(4), pp. 518–535.
[7] Bažant, Z. P., 1997, "Scaling of Quasibrittle Fracture: Asymptotic Analysis," Int. J. Fract., **83**(1), pp. 19–40.
[8] Bažant, Z. P., 2002, *Scaling of Structural Strength*, 2nd ed., Elsevier, London, UK.
[9] Bažant, Z. P., 2004, "Scaling Theory for Quasibrittle Structural Failure," Proc. Natl. Acad. Sci. U.S.A., **101**(37), pp. 13400–13407.
[10] RILEM Committee TC QFS, 2004, "Quasibrittle Fracture Scaling and Size Effect—Final Report," Mater. Struct., **37**(272), pp. 547–586.
[11] Melograna, J. D., and Grenested, J. L., 2002, "Adhesion of Stainless Steel to Fiber Reinforced Vinyl-Ester Composite," J. Compos. Technol. Res., **24**(4), pp. 254–260.
[12] Bahei-El-Din, Y. A., and Dvorak, G. J., 2001, "New Designs of Adhesive Joints for Thick Composite Laminates," Compos. Sci. Technol., **61**, pp. 19–40.
[13] Dvorak, G. J., Zhang, J., and Canyurt, O., 2001, "Adhesive Tongue-and-Groove Joints for Thick Composite Laminates," Compos. Sci. Technol., **61**, pp. 1123–1142.
[14] Liu, D., and Fleck, N. A., 1999, "Scale Effect in the Initiation of Cracking of a Scarf Joint," Int. J. Fract., **95**, pp. 67–88.
[15] Grenestedt, J. L., and Hallstrom, S., 1997, "Crack Initiation From Homogeneous and Bi-Material Corners," ASME J. Appl. Mech., **64**(4), pp. 811–818.
[16] Groth, H. L., 1988, "Stress Singularities and Fracture at Interface Corners in Bonded Joints," Int. J. Adhes. Adhes., **8**(2), pp. 107–113.
[17] Malyshev, B. M., and Salganik, R. L., 1965, "The Strength of Adhesive Joints Using the Theory of Cracks," Int. J. Fract. Mech., **1**, pp. 114–128.
[18] Achenbach, J. D., Keer, L. M., Khetan, R. P., and Chen, S. H., 1979, "Loss of Adhesion at the Tip of an Interfacial Crack," J. Elast., **9**(4), pp. 397–424.
[19] Comninou, M., 1978, "The Interfacial Crack in a Shear Field," ASME J. Appl. Mech., **45**, pp. 287–290.
[20] Comninou, M., 1977, "The Interfacial Crack," ASME J. Appl. Mech., **44**, pp. 631–636.
[21] Rice, J. R., 1988, "Elastic Fracture Mechanics Concepts for Interface Cracks," ASME J. Appl. Mech., **55**, pp. 98–103.
[22] Hutchinson, J. W., Mear, M. E., and Rice, J. R., 1987, "Crack Paralleling an Interface Between Dissimilar Materials," ASME J. Appl. Mech., **55**, pp. 828–832.
[23] Suo, Z., 1990, "Singularities, Interfaces and Cracks in Dissimilar Anisotropic Media," Proc. R. Soc. London, Ser. A, **427**, pp. 331–358.
[24] Agrawal, A., and Karlsson, A. M., 2006, "Obtaining Model Mixity for a Bimaterial Interface Cracks Using the Virtual Crack Closure Technique," Int. J. Fract., **141**, pp. 75–98.
[25] Ritchie, R. O., Knott, J. F., and Rice, J. R., 1973, "On the Relation Between Critical Tensile Stress and Fracture Toughness in Mild Steel," J. Mech. Phys. Solids, **21**, pp. 395–410.
[26] Kosai, M., Kobayashi, A. S., and Ramulu, M., 1993, "Tear Straps in Airplane Fuselage," *Durability of Metal Aircraft Structures*, Atlanta Technology, Atlanta, GA, pp. 443–457.
[27] Bažant, Z. P., and Yu, Q., 2006, "Size Effect on Strength of Quasibrittle Structures With Reentrant Corners Symmetrically Loaded in Tension," J. Eng. Mech., **132**(11), pp. 1168–1176.
[28] Bažant, Z. P., and Planas, J., 1998, *Fracture and Size Effect in Concrete and Other Quasibrittle Materials*, CRC, Boca Raton, FL.
[29] Tang, T., Bažant, Z. P., Yang, S., and Zollinger, D., 1996, "Variable-Notch One-Size Test Method for Fracture Energy and Process Zone Length," Eng. Fract. Mech., **55**(3), pp. 383–404.
[30] Bažant, Z. P., Caner, F. C., Le, J.-L., and Yu, Q., 2008, "Scaling of Strength of Metal-Composite Joints," *Proceedings of the 49th AIAA/ASME/ASCE/AHS/ASC Structures, Structural Dynamics and Materials Conference*, Schaumburg, IL, Apr. 7–10, Paper No. 2093.
[31] Godwin, E. W., 2000, "Tension," *Mechanical Testing of Advanced Fiber Composites*, J. M. Hodgkinson, ed., CRC, Boca Raton, FL, pp. 43–74.
[32] Broughton, W. R., 2000, "Through-Thickness Testing," *Mechanical Testing of Advanced Fiber Composites*, J. M. Hodgkinson, ed., CRC, Boca Raton, FL, pp. 143–169.
[33] Bažant, Z. P., and Cedolin, L., 1991, *Stability of Structures: Elastic, Inelastic, Fracture and Damage Theories*, Oxford University, New York.
[34] Le, J.-L., Bažant, Z. P., and Yu, Q., 2010, "Scaling of Strength of Metal-Composite Joints—Part II: Interface Fracture Analysis," ASME J. Appl. Mech., **77**, p. 011012.
[35] Beghini, A., Cusatis, G., and Bažant, Z. P., 2008, "Spectral Stiffness Microplane Model for Quasibrittle Composite Laminates—Part II: Calibration and Validation," ASME J. Appl. Mech., **75**(2), p. 021010.

Jia-Liang Le

Graduate Research Assistant
Department of Civil and Environmental
Engineering,
Northwestern University,
2145 Sheridan Road,
Evanston, IL 60208
e-mail: jialiang-le@northwestern.edu

Zdeněk P. Bažant[1]

McCormick Institute Professor and W. P. Murphy
Professor
Departments of Civil Engineering and Materials
Science,
Northwestern University,
2145 Sheridan Road, CEE/A135,
Evanston, IL 60208
e-mail: z-bazant@northwestern.edu

Qiang Yu

Postdoctoral Researcher
Department of Civil and Environmental
Engineering,
Northwestern University,
2145 Sheridan Road,
Evanston, IL 60208
e-mail: qiangyu@northwestern.edu

Scaling of Strength of Metal-Composite Joints—Part II: Interface Fracture Analysis

The effect of the size of hybrid metal-composite joint on its nominal strength, experimentally demonstrated in the preceding paper (part I), is modeled mathematically. Fracture initiation from a reentrant corner at the interface of a metallic bar and a fiber composite laminate sheet is analyzed. The fracture process zone (or cohesive zone) at the corner is approximated as an equivalent sharp crack according to the linear elastic fracture mechanics (LEFM). The asymptotic singular stress and displacement fields surrounding the corner tip and the tip of an interface crack emanating from the corner tip are calculated by means of complex potentials. The singularity exponents of both fields are generally complex. Since the real part of the stress singularity exponent for the corner tip is not $-\frac{1}{2}$, as required for finiteness of the energy flux into the tip, the interface crack propagation criterion is based on the singular field of the interface crack considered to be embedded in a more remote singular near-tip field of the corner from which, in turn, the boundaries are remote. The large-size asymptotic size effect on the nominal strength of the hybrid joint is derived from the LEFM considering the interface crack length to be much smaller than the structure size. The deviation from LEFM due to finiteness of the interface crack length, along with the small-size asymptotic condition of quasiplastic strength, allows an approximate general size effect law for hybrid joints to be derived via asymptotic matching. This law fits closely the experimental results reported in the preceding paper. Numerical validation according to the cohesive crack model is relegated to a forthcoming paper. [DOI: 10.1115/1.3172152]

1 Introduction

The preceding first part of this study [1] presented experimental evidence of a strong size effect on the strength of hybrid joints of metal to polymer-fiber composite. The objective of the second part is a mathematical analysis of the observed size effect.

In the past four decades, extensive analytical studies have been devoted to the effect of structure size on the strength of structures made of quasibrittle materials. These are brittle heterogeneous materials, which include concrete, as the archetypical case, fiber composites, sea ice, rocks, tough ceramics, stiff cohesive soils, rigid foams, wood, paper, bone, etc., and all brittle materials on a sufficiently small scale. In quasibrittle structures, the maximum load is reached after a stable development of either a large crack, or a large fracture process zone (FPZ) with distributed cracking. The latter case leads to Type 1 energetic size effect, which transits in the large-size limit to the Weibull statistical size effect. In the former case, the pre-existing crack is approximately equivalent to a notch, which leads to Type 2 energetic size effect [2,3].

Williams' solution [4] showed the dependence of the stress singularity exponent on the angle of a corner in a homogeneous body. A general approximate size effect law was recently derived for fracture emanating from a reentrant corner of arbitrary angle, provided that the loading is symmetric and the body is homogeneous and isotropic [5]. This size effect formulation now needs to be extended to a corner at the interface between two different materials, one of which is orthotropic. Compared with a reentrant corner in a homogeneous material, the analysis of a reentrant bi-material corner is complicated by the fact that the stress singularity exponent can be a complex number if the material mismatch is severe enough.

The size effect is defined for geometrically similar structures and represents the effect of structure size D (or characteristic dimension) on a load parameter of the dimension of stress. This parameter is normally chosen as the nominal strength, which is defined as $\sigma_N = P_{\max}/bD$, where $P_{\max}$ = maximum load, b = width of the structure (in the third dimension), and D = characteristic dimension, which may be chosen arbitrarily since only the ratio of σ_N values matters. Here we chose D = interface length (Fig. 1(a)). To avoid small secondary effects of the length of crack front edge in the third dimension (stemming from a transition from plane strain to plane stress along the edge), it is better to consider two-dimensional similarity, i.e., b = constant.

According to elasticity with strength limit, nonsoftening plasticity or any theory in which the material failure criterion is characterized solely in terms of stresses and strains, σ_N is independent of structure size D [6,7,2] when geometrically similar structures are compared. Any deviation from this classical situation is called the size effect. The Weibull statistical size effect is negligible when the FPZ or the crack length at failure is large, and also when the crack can initiate at one point only (the corner). Therefore, the size effect in the joints is energetic (i.e., nonstatistical), being caused by the presence of material fracture energy G_f or material characteristic length l_0 in the material failure criterion.

Similar to the previous size effect analysis for many other quasibrittle structures [5,2,3,8,9], the size effect law will be asymptotically anchored at the large-size limit in linear elastic fracture mechanics (LEFM). The transition to small-size behavior and extension to various corner angles in the joint will be approximated by asymptotic matching. For reentrant corners (or V-notches) in a homogeneous body, this kind of approach has already been shown to lead to good agreement with experiments [5].
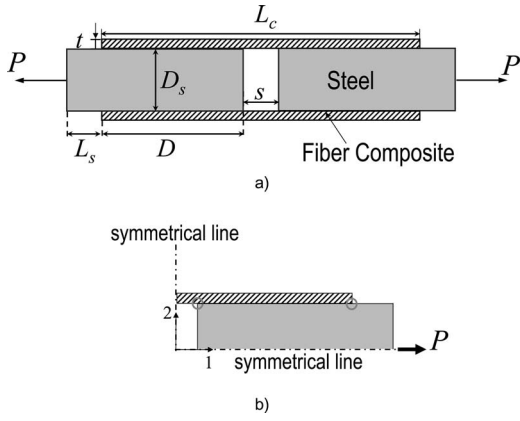

Fig. 1 Geometry of double-lap hybrid joint

2 Stress Singularity Exponent

In the double-lap joint considered here, both the structure and the loading are symmetric. Before the peak load is attained, the elastic field must be symmetric as well. Therefore, we analyze only one quarter of the specimen (Fig. 1(b)). In this quarter, there are two critical bimaterial corners where the corner geometry and material mismatch cause singularity and stress concentration. To identify the critical corner from which the crack propagates, the stress singularity exponents must be calculated.

The stress singularity exponents for bimaterial wedges have been extensively studied for isotropic materials [10,11]. For general orthotropic-orthotropic interfaces or orthotropic-isotropic interfaces, various numerical approaches, such as the finite difference method with eigenvalue analysis, and the finite element iterative method, have been used to determine the singularity exponent and the surrounding asymptotic elastic field [12–14].

In this study, an analytical approach using the complex field method is adopted to calculate the singularity for bimaterial wedges (shown in Fig. 2) [15]. Under plane loading condition, the elastic field in each layer of material (including the displacements, boundary tractions, and stress fields) may be represented by two holomorphic functions $f_1(z_1)$ and $f_2(z_2)$, where $z_j = x + \mu_j y$ ($j = 1,2$); μ_j is the root with positive imaginary part of the fourth order equation

$$\lambda \mu^4 + 2\rho \lambda^{1/2} \mu^2 + 1 = 0 \quad (1)$$

Here $\lambda = s_{11}/s_{22}$ and $\rho = 0.5(2s_{12} + s_{66})(s_{11}s_{22})^{-1/2}$; s_{ij} refers to the elements of the general material compliance matrix, and subscripts i and j refer to Cartesian coordinates $x_i (i = 1,2)$. When the conditions of equilibrium and compatibility are imposed and the singularity lies on the left side as the observer travels in the positive, or counterclockwise, direction of the arc, the corresponding displacement, stress, and resultant forces on the arc can be represented by these two functions as follows [16]:
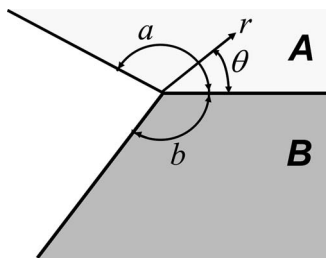

Fig. 2 Geometry of bimaterial wedge

$$u_i = 2 \ \mathrm{Re} \sum_{j=1}^{2} A_{ij} f_j(z_j) \quad (2)$$

$$\sigma_{2i} = 2 \ \mathrm{Re} \sum_{j=1}^{2} L_{ij} f_j'(z_j) \quad (3)$$

$$\sigma_{1i} = -2 \ \mathrm{Re} \sum_{j=1}^{2} L_{ij} \mu_j f_j'(z_j) \quad (4)$$

$$T_i = -2 \ \mathrm{Re} \sum_{j=1}^{2} L_{ij} f_j(z_j) \quad (5)$$

where matrices $\mathbf{A}$ and $\mathbf{L}$ are defined as

$$\mathbf{A} = \left\{ \begin{array}{cc} s_{11}\mu_1^2 + s_{12} & s_{11}\mu_2^2 + s_{12} \\ s_{21}\mu_1 + s_{22}/\mu_1 & s_{22}\mu_2 + s_{22}/\mu_2 \end{array} \right\} \quad (6)$$

$$\mathbf{L} = \left\{ \begin{array}{cc} -\mu_1 & -\mu_2 \\ 1 & 1 \end{array} \right\} \quad (7)$$

Near the corner tip, the displacement field as a function of polar coordinates (r, θ) (Fig. 2) may be assumed to be separable, and the dependence on radial coordinate r to be a power law of some exponent δ, which can be either real or complex. The corresponding stress field has a singular term proportional to $r^{\delta-1}$. Hence, the complex potentials near the bimaterial corner tip may be expressed, for both materials, as follows [15]:

$$f_k(z_k) = \phi_k z_k^\delta = \phi_k r^\delta (\cos\theta + \mu_k \sin\theta)^\delta \quad (k = 1,2) \quad (8)$$

To write these potentials in a more compact form, we define for each material the vectors: $\mathbf{\Phi} = [\phi_1, \phi_2]^T$, $\mathbf{Z} = [z_1, 0; 0, z_2]$, and $\mathbf{F} = [f_1, f_2]^T$ (where T denotes a transpose). For each material, the corresponding displacements and resultant forces can be written in the matrix form as

$$\mathbf{u} = [u_1, u_2]^T = \mathbf{A} \cdot \mathbf{F} + \overline{\mathbf{A}} \cdot \overline{\mathbf{F}} = \mathbf{A} \cdot \mathbf{Z}^\delta \cdot \mathbf{\Phi} + \overline{\mathbf{A}} \cdot \overline{\mathbf{Z}}^\delta \cdot \overline{\mathbf{\Phi}} \quad (9)$$

$$-\mathbf{T} = [-T_1, -T_2]^T = \mathbf{L} \cdot \mathbf{F} + \overline{\mathbf{L}} \cdot \overline{\mathbf{F}} = \mathbf{L} \cdot \mathbf{Z}^\delta \cdot \mathbf{\Phi} + \overline{\mathbf{L}} \cdot \overline{\mathbf{Z}}^\delta \cdot \overline{\mathbf{\Phi}}$$
$$(10)$$

where the overbar denotes the conjugate of a complex matrix.

Finally, one needs to impose the boundary conditions: a traction-free exterior boundary ($\theta = a, -b : \mathbf{T} = 0$); and the continuity of displacements and tractions at the interface between two materials; $\theta = 0$: $\mathbf{T}_A = \mathbf{T}_B$ and $\mathbf{u}_A = \mathbf{u}_B$. This results in a system of linear equations, with the matrix form

$$\mathbf{K}(\delta)\nu = \begin{bmatrix} \mathbf{Y_A} & \mathbf{1} & \mathbf{0} & \mathbf{0} \\ \mathbf{0} & \mathbf{0} & \mathbf{Y_B} & \mathbf{1} \\ \mathbf{1} & \mathbf{1} & -\mathbf{1} & -\mathbf{1} \\ \mathbf{B_A} & -\overline{\mathbf{B}}_\mathbf{A} & -\mathbf{B_B} & -\overline{\mathbf{B}}_\mathbf{B} \end{bmatrix} \left\{ \begin{array}{c} (\mathbf{L\Phi})_A \\ \overline{(\mathbf{L\Phi})}_A \\ (\mathbf{L\Phi})_B \\ \overline{(\mathbf{L\Phi})}_B \end{array} \right\} = 0 \quad (11)$$

where $\mathbf{1} = [1,0;0,1]$ and $\mathbf{0} = [0,0;0,0]$. Submatrices $\mathbf{Y}_k$ and $\mathbf{B}_k$ (where $k = A, \ B = $ labels of materials A and B) are defined as

$$\mathbf{Y}_k = \overline{\mathbf{L}}_k [\overline{\mathbf{Z}}_k(\theta_k)]^{-\delta} \overline{\mathbf{L}}_k^{-1} \mathbf{L}_k [\mathbf{Z}_k(\theta_k)]^\delta \mathbf{L}_k^{-1} \quad (12)$$

$$\mathbf{B}_k = i \mathbf{A}_k \mathbf{L}_k^{-1} \quad (13)$$

where $i^2 = -1$. It may be noted that the submatrix $\mathbf{Y}_k$ defined above cannot be directly applied to isotropic materials ($\mu_k = i$) because $\mathbf{L}_k$ is not invertible. However, one can calculate $\mathbf{Y}_k$ by taking the limit of $\mu_k \to i$ ($\mathbf{B}_k$ is well defined for isotropic materials) [15,17]. The displacement singularity δ must be solved from the condition $\det(\mathbf{K}) = 0$. To solve it numerically, it is the easiest to seek the value of δ for which the condition number of matrix $\mathbf{K}$ becomes very large.
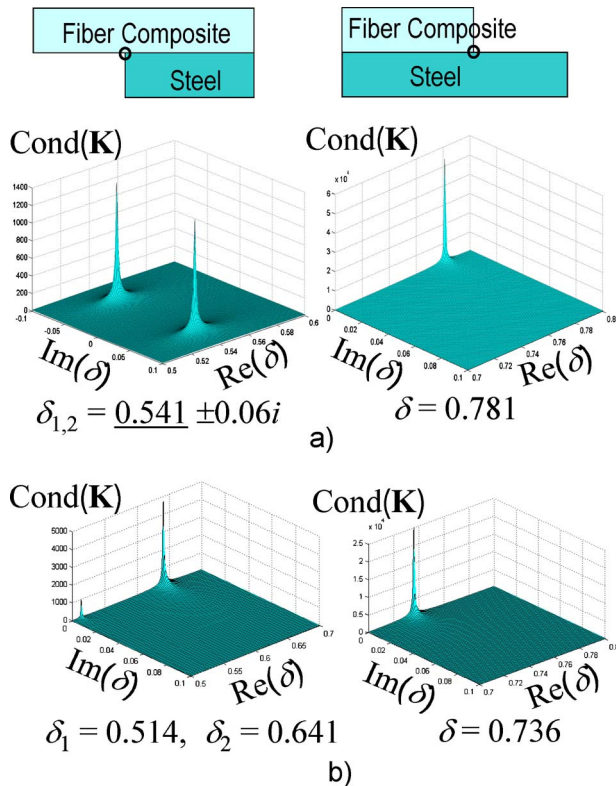
Fig. 3 Exponent of displacement singularity of hybrid joint: (*a*) test series I and II and (*b*) test series III

Three test series have been reported in the preceding paper [1]. The orthotropic elastic constants of the fiber composite used in test series I and II are $E_1 = 30$ GPa, $E_2 = 9.5$ GPa, $\nu_{12} = 0.2$, and $G_{12} = 3.0$ GPa. The elastic constants of composite used in test series III are $E_1 = 125.5$ GPa, $E_2 = 9.0$ GPa, $\nu_{12} = 0.3$, and $G_{12} = 5.6$ GPa. For steel, which is isotropic, $E = 200$ GPa and $\nu = 0.3$. Figure 3 shows in the complex plane the plot of $\det(\mathbf{K})$ for the displacement singularity. For the joint used in test series I and II, the displacement field at the left corner (at which the stiffer material terminates) is found to exhibit singularities with exponents being a pair of complex conjugates $\delta = 0.541 \pm 0.06i$ and, at the right corner (at which the softer material terminates), a real displacement singularity $\delta = 0.781$. For the joint used in test series III, the displacement at the left corner exhibits two real displacement singularities: $\delta_1 = 0.514$ and $\delta_2 = 0.641$, while at the right corner there is a real displacement singularity with $\delta = 0.736$. So, for all the joints tested, the singularity at the left corner is much stronger than it is at the right corner. Hence, the crack is expected to start propagating from the left corner, which agrees with the experimental observations [1]. The left corner is that which governs the strength of the hybrid joint, and so the fracture needs to be investigated only for that corner.

3 Fracture of Bimaterial Corner and Size Effect Law Asymptote

Various fracture criteria have been proposed to characterize the crack initiation for general bimaterial corners [18–20]. Due to the nature of mix-mode fracture at bimaterial corner, the use of stress intensity factors as a fracture criterion generally necessitates an empirical equation involving the stress intensity factors for different modes [21]. As an empirical approach to certain situations, such as bimaterial butt joints, one may simply use a critical value of the stress intensity factor as a fracture criterion [22–24]. A more general and effective approach is to consider the energy release rate or the corresponding fracture energy as the failure criterion [25].

Consider a bimaterial corner with the strongest stress singularity $\lambda = \kappa \pm i\eta$. The corresponding near-tip stress field can be written as

$$\sigma_{ij} = \text{Re}[Hr^{i\eta}\alpha_{ij}(\theta)]r^{\kappa} \qquad (14)$$

where H is the stress intensity factor, and α_{ij} is the distribution of stress. Both of them are complex, in general. Dimensional analysis shows that H must have the form

$$H = \frac{P}{bD}D^{-\kappa}|h(\eta,\varphi)|e^{i(\omega - \eta \ln D)} \qquad (15)$$

where P is the applied load, b is the width of the joint, D is the characteristic size of the joint (chosen as the interface length), $h(\eta,\varphi)$ is the dimensionless complex stress intensity factor, φ is the effective loading angle (which combines the effects of loading angle and boundary conditions), and ω is the phase angle of $h(\eta,\varphi)$.

For a general bimaterial wedge, the exponents of displacement singularities can be either a pair of complex conjugates, a single real number or two unequal real numbers depending on the degree of material mismatch and the geometry. For the former two cases, Eq. (14) represents the entire singular stress field [19,26], while for the latter case, Eq. (14) represents only the singular stress field corresponding to the strongest stress singularity. The entire singular stress zone may be written as $\sigma_{ij} = H_1 r^{\kappa_1}\alpha_{ij}(\theta) + H_2 r^{\kappa_2}\beta_{ij}(\theta)$. For symmetric structures made of homogenous materials, κ_1 and κ_2 correspond to the symmetric and antisymmetric modes of fracture (Modes I and II) (the simplest example is the homogenous reentrant corner analyzed in Ref. [5]). Depending on the loading, it is possible that only one of them governs the entire stress field.

Because of the lack of symmetry of bimaterial joints, the symmetric and antisymmetric modes do not exist, and κ_1 and κ_2 always coexist. Many studies showed the importance of considering both singularities to properly obtain the entire singular stress field for a bimaterial joint [21,27,28]. Nevertheless, for the large-size asymptotic size effect, only the singular stress field corresponding to the strongest singularity is relevant. So, in what follows, only the corner tip singular field corresponding to the strongest stress singularity is considered.

Once the crack initiates from the corner tip, it will propagate along the path that corresponds to the highest energy release rate or the lowest fracture energy dissipation. The adhesive layer connecting the fiber composite and the steel is as thin as possible and is generally much weaker than both materials in normal hybrid joint designs. So, the crack is expected to propagate along the interface.

The initiation of a crack, or macrocrack, requires formation of a microcracking zone of a certain finite characteristic length l_{FPZ} within (and possibly near) the adhesive layer. This zone, called the fracture process zone (FPZ), develops stably and transmits cohesive stresses. As soon as the full FPZ develops, the maximum load is attained. After that, the equilibrium load is expected to decrease, which requires the geometry to be positive [9], i.e., the stress intensity factor to increase with the crack length when the load is constant. A positive geometry is normally satisfied but, of course, needs to be verified.

In analogy to the derivation of the size effect law for cracks in homogenous solids [2], we may assume that, not too close to the FPZ, the effect of a finite-size FPZ on the elastic field is approximately equivalent to the effect of an interface crack, whose length c_f is proportional to length l_{FPZ} of the FPZ, and is roughly $l_{\text{FPZ}}/2$ [2,9,29]. Therefore, what matters at maximum load is the asymptotic field close (but not too close) to an interfacial crack, rather than to a corner. It has been shown [17] that the stress singularity exponent of an interfacial crack must have the form
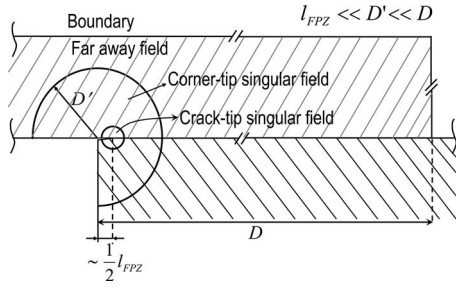
Fig. 4 Interfacial crack embedded in the singular near-tip field of corner

$$\lambda_{\text{crack}} = -\tfrac{1}{2} + i\eta' \tag{16}$$

In the foregoing, a distinction is made among (1) the near-tip asymptotic field of the imagined effective crack assumed to have a similar global effect as the actual FPZ; (2) the near-tip field of the corner prevailing not too close to the tip of the crack so that it can envelop the near-tip field of the crack; and (3) the far-away field affected by the boundary conditions (Fig. 4). These three fields are here matched energetically, through the strength of the singularities. Note that the second field corresponds to what has been conceived as the intermediate asymptotic—an important concept conceived and rigorously developed by Barenblatt [30,31], which has apparently not yet been used in fracture mechanics.

The intermediate asymptotic is attained if $D \gg D' \gg l_{\text{FPZ}}$ (where D' is the size of the corner tip singular field), and the near-tip field of a crack is applicable only if the radial distance from the crack tip $r \ll l_{\text{FPZ}}$ (Fig. 4), i.e., in the large-size asymptotic limit. In this limit, the asymptotic near-tip field of the hypothetical interfacial crack of length c_f, substituted for the FPZ, must be surrounded by the singular stress field of a bimaterial corner tip corresponding to the strongest stress singularity (except if the laminate thickness were too small, which has been checked not to occur in practical situations). Therefore, the stress intensity factor K at the interfacial crack tip will depend on the stress field, whose magnitude is characterized by the stress intensity factor H of the corner tip. By dimensional analysis, the two stress intensity factors may be related as follows [19,22]:

$$Kc_f^{i\eta'} = Hc_f^{\kappa+0.5}c_f^{i\eta}\zeta \tag{17}$$

where ζ is the dimensionless complex number. Such a relation has been analytically derived for the case of a crack emanating from a homogeneous notch tip [32,33]. For the interfacial crack, the near-tip stresses on the crack line ahead of the tip and the opening displacements (or crack face separations) behind the tip can be expressed as [17,34]

$$\alpha\sigma_{yy} + i\sigma_{xy} = K(2\pi r)^{-1/2}r^{i\eta'} \tag{18}$$

$$\alpha^{-1}\delta_y + i\delta_x = \frac{K}{E}(r/2\pi)^{1/2}r^{i\eta'}m \tag{19}$$

where $\delta_i = u_i(-r, 0^+) - u_i(-r, 0^-) =$ displacement jump behind the crack tip, m is the dimensionless complex number characterizing the geometry of the structure, E is any one of the elastic moduli of either material, and α is the constant reflecting the material orthotropy.

The energy release rate $\mathcal{G}$ represents the energy flux into the crack tip. The flux can be obtained as the work required for the crack to advance by an infinitesimal distance, Δ, divided by Δ. Therefore,

$$\mathcal{G} = \lim_{\Delta\to 0}\frac{1}{2\Delta}\int_0^\Delta [\sigma_{yy}(x)\delta_y(\Delta-x) + \sigma_{xy}(x)\delta_x(\Delta-x)]\mathrm{d}x \tag{20}$$

Noting Eqs. (18) and (19) and introducing the dimensionless variable $\xi = x/\Delta$, one obtains

$$\mathcal{G} = \frac{|K|^2|m|}{2E}\int_0^1 \sqrt{\frac{1-\xi}{\xi}}\cos\left[\eta'\ln\left(\frac{1-\xi}{\xi}\right) + \psi\right]\mathrm{d}\xi \tag{21}$$

The foregoing integral can be shown to be a constant [35,36]. Therefore, the energy release rate function for an interfacial crack can be always written as

$$\mathcal{G} = \frac{CK\bar{K}}{E} \tag{22}$$

Upon substituting Eqs. (17) and (15) into the foregoing equation, one obtains

$$\mathcal{G} = \frac{\sigma^2 D^{-2\kappa}}{Ec_f^{-1-2\kappa}}|g|^2 \tag{23}$$

where $\sigma =$ nominal stress $= P/bD$ and $|g| = C|\zeta||h|$. Within the LEFM framework, a crack can propagate once $\mathcal{G}$ reaches a certain critical value G_f, called the fracture energy, and this also represents the condition of maximum load P. From Eq. (23), one obtains the LEFM expression of nominal strength $\sigma_N(=P_{\max}/bD)$ of the bimaterial joint

$$\sigma_N = |g|^{-1}\sqrt{EG_f}c_f^{-\kappa-0.5}D^\kappa \tag{24}$$

This equation represents the large-size asymptote of the size effect law. Clearly, this asymptote is a power scaling law, with an exponent directly related to the real part of the exponent of the strongest stress singularity at the bimaterial corner.

Evidently, Eq. (24) applies to fracture of a certain single mode. Let us now rewrite this equation for the case of a reentrant corner made of a homogenous material under symmetric tensile loadings, which is mode I fracture. In this case, only one real stress singularity governs the entire singular stress field (for a homogeneous reentrant corner under general loading conditions, there are two unequal real stress singularities, which correspond to symmetric and asymmetric fracture modes). The effective size of FPZ can be expressed as $c_f = \gamma l_0$, in which $l_0 = EG_f/f_t'^2 =$ Irwin's characteristic length. Equation (24) may then be written in an alternative form

$$\sigma_N = f_t'k(D/c_f)^\kappa \tag{25}$$

where $k = (|g|\sqrt{\gamma})^{-1}$, and f_t' is the tensile strength of the material. This equation has the same form as the large-size asymptote of the general size effect law for a reentrant corner under symmetric tensile loading (Eq. (16) in Ref. [5]), which has recently been derived on the basis of the strength criterion; i.e., the peak load is attained when the tensile stress at the center of FPZ reaches the material tensile strength. The equivalence between Eqs. (25) and (16) in Ref. [5] is to be expected, since the strength criterion for single-mode fracture must be a special case of the present energy criterion.

4 General Size Effect Law Via Asymptotic Matching

A general approximate formula for the size effect on the nominal strength σ_N, spanning all the sizes and a range of corner angles, can be obtained through asymptotic matching [2]. The geometry of a hybrid joint with various corner angles is shown in Fig. 5.

A general approximate size effect equation has recently been developed for symmetrically loaded reentrant corners in homogenous materials of various corner angles. In that case, the entire singular stress field is governed solely by one real stress singularity [5]. For the general case of bimaterial joints in which the singularities are either a pair of complex conjugates or two un-
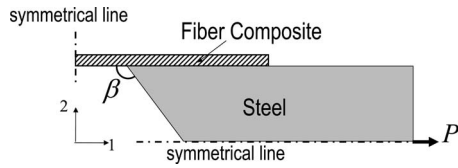
Fig. 5 General geometry of hybrid joint with varying joint angle

Fig. 6 (*a*) **Finite element model of hybrid joint and** (*b*) **finite element model of ancillary boundary layer problem**

equal real numbers, the aforementioned analysis shows that only the real part of the strongest singularity exponent matters for the energy release rate at the large size limit. Therefore, an equation of similar type can be used to approximate the general size effect law for the hybrid joint

$$\sigma_N = \sigma_0 \left(1 + \frac{D}{D_{0\beta}}\right)^{\kappa(\beta)} \quad (26)$$

where σ_0 and $D_{0\beta}$ are parameters yet to be determined, κ is the real part of the exponent of the strongest stress singularity at the bimaterial corner, which is a function of corner angle β. The foregoing equation has been set up to match the following three essential asymptotic conditions.

(1) For $D/l_0 \to 0$, there must be no size effect since the FPZ occupies the whole structure (what matters in that case is solely the material strength, and not the energy release because the failure is quasiplastic).
(2) For $D/l_0 \to \infty$, Eq. (26) must match Eq. (24) as the large-size asymptote of the size effect law.
(3) For $\beta \to \pi$ (smooth surface, no corner), the size effect of this type must vanish (in that case, a cohesive crack initiates from a smooth surface, which leads to another type of size effect, Type 1 [2,3,37], which does not represent the limit case of the present size effect).

Note that the foregoing equation does not apply for the limiting case $\beta \to 0$. It is found that, in this limit, the structure may have a negative geometry (i.e., the derivative of the energy release rate function with respect to the crack length at constant load is negative). In that case, the maximum load does not occur at crack initiation, since the crack grows stably at increasing load, and the size effect is different (known as Type 3 size effect law [2,3]).

On the other hand, Eq. (26) for $\beta \to \pi$ does not continuously approach the Type 1 size effect law either. A generalization would be needed to describe the transition to Type 3 size effect law [3] (for $\beta \to 0$) and to Type 1 size effect (for $\beta \to \pi$).

By matching asymptotic condition 2 for arbitrary corner angles, one further obtains

$$\frac{\sigma_0(\beta)}{D_{0\beta}^{\kappa}} = \frac{\sqrt{EG_f(\beta)}}{|g(\beta)|c_f^{\kappa+0.5}} \quad (27)$$

Parameters $\sigma_0(\beta)$ and $D_{0\beta}$ can be easily obtained by calibrating the model on the basis of available size effect data. Nevertheless, it is impossible to obtain the fracture toughness, $G_f(\beta)$, and the effective size of FPZ, c_f, since, for a certain joint angle, there is only one matching condition involving these two fracture parameters. Note that, in general, the fracture toughness $G_f(\beta)$ can vary with the joint angle β due to mode mixity. The dependence of G_f on the mode mixity can be expressed as [17,34]

$$G_f = F(G_I, G_{II}, \phi) \quad (28)$$

where G_I and G_{II} denote the mode I and mode II fracture toughness. Phase angle ϕ, characterizing the degree of mode mixity, is defined for interfacial crack problems as [17,34,38]
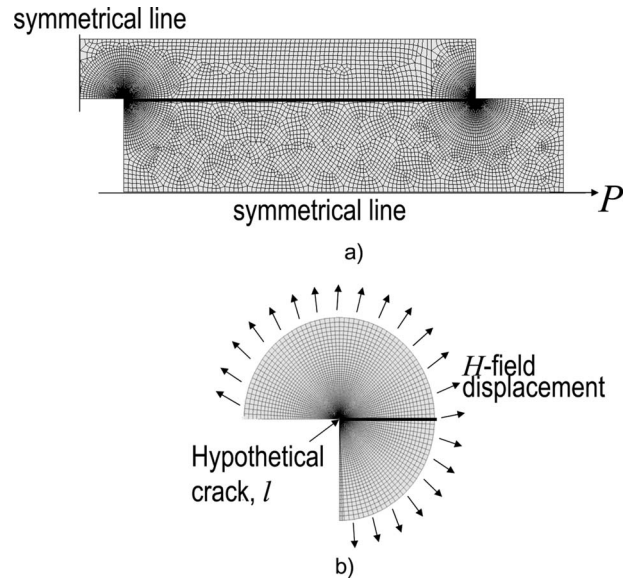
$$\phi = \tan^{-1}\left[\frac{\operatorname{Im}(Kl^{i\eta'})}{\operatorname{Re}(Kl^{i\eta'})}\right] \quad (29)$$

where l is an arbitrary length scale, which might be chosen as the fracture process zone size (or multiple of atomic dimensions [38]). The stress intensity factor for the interfacial crack K is given by Eq. (17). The dimensionless complex number ζ in Eq. (17) depends on the geometry [21,22]. Hence, the phase angle ϕ varies with the geometry (joint angle). Therefore, these two fracture parameters, G_f and c_f, cannot be determined merely by fitting of the experimental size effect data, even if two sets of size effect data for two different joint angles are considered.

To overcome this obstacle, G_f needs to be estimated by numerical simulation with the cohesive crack model [39], where the cohesive law may be calibrated by the available experimental size effect data reported in the preceding paper [1]. Then the effective fracture process zone size c_f can be obtained from Eq. (27).

5 Numerical Evaluation of Model Parameters

In the foregoing calibration by Eq. (27), the model parameter $|g|$ needs to be determined by finite element analysis. To illustrate the numerical procedure, let us consider the joint used in test series II. In the numerical model, all the elastic moduli of the composite are normalized relative to the elastic modulus of steel, taken as $E = E(\text{steel}) = 1$, and the applied force P and the characteristic dimension D are chosen as 1.

Parameter $|g|$ can be obtained by calculating the energy release rate at the tip of the interfacial crack, which lies well within the singular stress field characterized by H. This parameter can be calculated in two steps, as follows.

First, the singular stress zone is obtained by finite element analysis of the joint. In the linear elastic finite element model, eight-node quadrilateral elements are used for both materials, as shown in Fig. 6(*a*). To obtain the singular field, normally expressed in polar coordinates, the regions near the bimaterial corners are meshed by numerous rings of elements, which are progressively refined on approach to the tip so that the ratio between the smallest and largest element sizes is about 1: 100.

Figure 7 shows, in the logarithmic scale, the profiles of magnitude of normal and shear stress ($\sigma_{\theta\theta}$ and $\sigma_{r\theta}$) along the interface, for both corners. For the left corner of the joint (Fig. 7(*a*)), the slopes of the asymptotes of $|\sigma_{\theta\theta}|$ and $|\sigma_{r\theta}|$ in the logarithmic scale
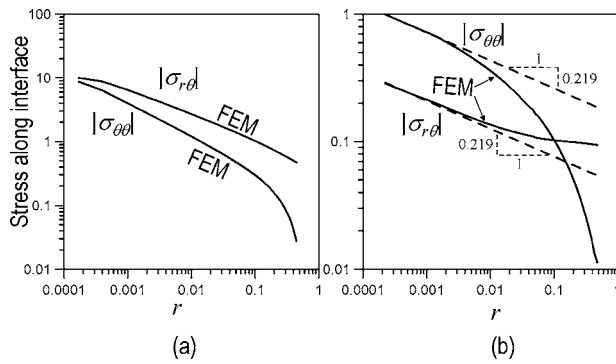
Fig. 7 Normal and shear stress along the interface: (*a*) left corner and (*b*) right corner

Fig. 8 Energy release rate at the hypothetical interfacial crack tip

plot are not the same. This difference is due to the fact that the exponent of stress singularity at this corner is complex. The asymptotic stress field is given by Eq. (14), which can further be expressed as

$$\sigma_{ij} = |H||\alpha_{ij}(\theta)|r^{\kappa}\cos(\vartheta_{ij} + \eta \ln r) \qquad (30)$$

It is obvious that the dependence of σ_{ij} on r is not a simple power law. Due to the unknown variable ϑ_{ij}, which characterizes the mode mixity, it is impossible to determine the complex exponent of stress singularity simply by matching the stress profile along the interface only, and so the reach of the singular stress zone is not known. As for the stress profile oscillation, which must occur sufficiently close to the corner tip, its region is normally very small due to the very small value of the imaginary part η. It is for this reason that this oscillation is not generally reflected in finite element results.

At the right corner of the joint, the asymptotes of $|\sigma_{\theta\theta}|$ and $|\sigma_{r\theta}|$ are seen to have the same slope (Fig. 7(*b*)). This indicates that the stress singularity at that corner must be real and the near-tip stress field is given by $\sigma_{ij} = Hr^{\kappa}\alpha_{ij}(\theta)$ [26]. By matching the asymptotic stress field, the stress singularity exponent is found to be -0.219, and so the corresponding displacement singularity exponent is 0.781. This validates the previous calculations made by the complex potential method.

Second, one needs to solve an ancillary boundary layer problem which couples the inner stress field caused by the interfacial crack to the outer singular H-field. The boundary layer problem consisting of a semicircular region (fiber composite) and a quartercircular region (steel) (Fig. 6(*b*)) is subjected to displacements of the asymptotic H-field, which can be directly obtained from the FEM analysis in the step 1. Since the exact reach of the H-field is not determined, the H-field displacement is extracted at a reasonably small radius ($r/D \approx 0.01$). The interfacial crack length l is chosen to be very small compared with the dimension of the boundary layer. This ensures the crack to lie well within the H-field. The energy release rate $\mathcal{G}$ at the interfacial crack tip is directly calculated via the J-integral using the commercial FEM software ABAQUS [40]. When the loading, dimension, and elastic constants are normalized, one may rewrite Eq. (23) as follows:

$$\log \mathcal{G} = (1 + 2\kappa)\log(l) + 2\log|g| \qquad (31)$$

Upon considering various small crack lengths l, one obtains the relationship between log $\mathcal{G}$ and log l (Fig. 8). It is seen to follow a straight line, whose slope is 0.082. This agrees well with the value of $(1 + 2\kappa)$. One can then easily obtain the value $|g| = 1.042$.

6 Conclusions

With the help of asymptotic matching, a general approximate size effect law for the strength of hybrid metal-composite joints
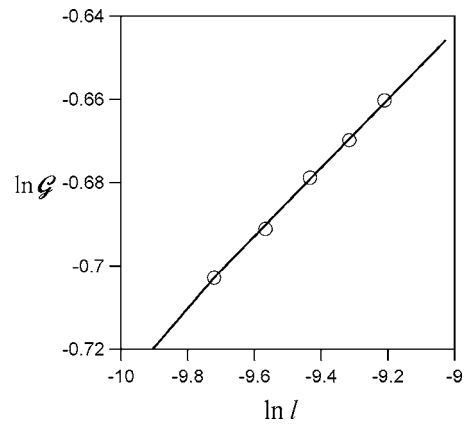
can be derived from the near-tip asymptotic stress fields of a bi-material corner and of an interface crack emanating from this corner.

The size effect law derived is validated by comparison with size effect experiments on metal-composite joints with two kinds of fiber-polymer composites.

The size effect in hybrid joints is quite strong. Thus it is unsafe to design large hybrid joints on the basis of classical material failure criteria expressed in terms of stresses or strains, or both.

Neither it is safe to extrapolate from small-scale laboratory tests of hybrid joints to large structure sizes without considering the size effect.

References
[1] Yu, Q., Bažant, Z. P., Bayldon, J., Le, J.-L., Caner, F. C., Ng, W. H., Waas, A. M., and Daniel, I. M., (2010), "Scaling of Strength of Metal-Composite Joints—Part I: Experimental Investigation," ASME J. Appl. Mech., **77**, p. 011011.
[2] Bažant, Z. P., 2005, *Scaling of Structural Strength*, 2nd ed., Elsevier, London.
[3] Bažant, Z. P., 2004, "Scaling Theory for Quasibrittle Structural Failure," Proc. Natl. Acad. Sci. U.S.A., **101**(37), pp. 13400–13407.
[4] Williams, M. L., 1952, "Stress Singularities Resulting From Various Boundary Conditions in Angular Corners of Plates in Extension," ASME J. Appl. Mech., **74**, pp. 526–528.
[5] Bažant, Z. P., and Yu, Q., 2006, "Size Effect on Strength of Quasibrittle Structures With Reentrant Corners Symmetrically Loaded in Tension," J. Eng. Mech., **132**(11), pp. 1168–1176.
[6] Bažant, Z. P., 1984, "Size Effect in Blunt Fracture: Concrete, Rock, Metal," J. Eng. Mech., **110**(4), pp. 518–535.
[7] Bažant, Z. P., 1993, "Scaling Laws in Mechanics of Failure," J. Eng. Mech., **119**(9), pp. 1828–1844.
[8] Bažant, Z. P., 1997, "Scaling of Quasibrittle Fracture: Asymptotic Analysis," Int. J. Fract., **83**(1), pp. 19–40.
[9] Bažant, Z. P., and Planas, J., 1997, *Fracture and Size Effect in Concrete and Other Quasibrittle Materials*, CRC, Boca Raton, FL.
[10] Bogy, D. B., 1971, "Two Edge-Bonded Elastic Wedges of Different Materials and Wedge Angles Under Surface Tractions," ASME J. Appl. Mech., **38**, pp. 377–385.
[11] Hein, V. L., and Erdogan, F., 1971, "Stress Singularities in a Two-Material Wedge," Int. J. Fract. Mech., **7**, pp. 317–330.
[12] Achenbach, J. D., Bažant, Z. P., and Khetan, R. P., 1976, "Elastodynamic Near-Tip Fields for a Crack Propagating Along the Interface of Two Orthotropic Solids," Int. J. Eng. Sci., **14**, pp. 811–818.
[13] Barsoum, R. S., 1988, "Application of the Finite Element Iterative Method to the Eigenvalue Problem and a Crack Between Dissimilar Media," Int. J. Numer. Methods Eng., **26**, pp. 541–554.
[14] Barsoum, R. S., and Freese, C. E., 1984, "An Interative Approach for the Evaluation of Delamination Stresses in Laminated Composite," Int. J. Numer. Methods Eng., **20**, pp. 1415–1431.
[15] Desmorat, R., and Leckie, F. A., 1998, "Singularities in Bimaterials: Parametric Study of an Isotropic/Anisotropic Joint," Eur. J. Mech. A/Solids, **17**, pp.

33–52.

[16] Lekhnitskii, S. G., 1968, *Anisotropic Plates*, Gorden & Beach Science, London.

[17] Suo, Z., 1990, "Singularities, Interfaces and Cracks in Dissimilar Anisotropic Media," Proc. R. Soc. London, Ser. A, **427**, pp. 331–358.

[18] Gomez, F. J., and Elices, M., 2003, "A Fracture Criterion for Sharp V-Notched Samples," Int. J. Fract., **123**, pp. 163–175.

[19] Grenestedt, J. L., and Hallstrom, S., 1997, "Crack Initiation From Homogeneous and Bimaterial Corners," ASME J. Appl. Mech., **64**, pp. 811–818.

[20] Leguillon, D., 2002, "Strength or Toughness? A Criterion for Crack Onset at a Notch," Eur. J. Mech. A/Solids, **21**, pp. 61–72.

[21] Labossiere, P. E. W., Duun, M. L., and Cunningham, S. J., 2002, "Application of Bimaterial Interface Corner Failure Mechanics to Silicon/Glass Anodic Bonds," J. Mech. Phys. Solids, **50**, pp. 405–433.

[22] Liu, D., and Fleck, N. A., 1999, "Scale Effect in the Initiation of Cracking of a Scarf Joint," Int. J. Fract., **95**, pp. 67–88.

[23] Reedy, E. D., Jr., 1993, "Asymptotic Interface-Corner Solutions for Butt Tensile Joints," Int. J. Solids Struct., **30**(6), pp. 767–777.

[24] Reedy, E. D., Jr., 2000, "Comparison Between Interface Corner and Interfacial Fracture Analysis of an Adhesively-Bonded Butt Joint," Int. J. Solids Struct., **37**, pp. 2429–2442.

[25] Zhang, Z., and Suo, Z., 2007, "Split Singularities and the Competition Between Crack Penetration and Debond at a Bimaterial Interface," Int. J. Solids Struct., **44**, pp. 4559–4573.

[26] Banks-Sills, L., and Sherer, A., 2002, "A Conservative Integral for Determining Stress Intensity Factors of a Bimaterial Notch," Int. J. Fract., **115**, pp. 1–26.

[27] Liu, X. H., Suo, Z., and Ma, Q., 1998, "Split Singularities: Stress Field Near the Edge of a Silicon Die on a Polymer Substrate," Acta Mater., **47**(1), pp. 67–76.

[28] Munz, D., and Yang, Y. Y., 1993, "Stress Near the Edge of Bonded Dissimilar Materials Described by Two Stress Intensity Factors," Int. J. Fract., **60**, pp. 169–177.

[29] Bažant, Z. P., Zhou, Y., Daniel, I. M., Caner, F. C., and Yu, Q., 2006, "Size Effect on Strength of Laminate-Foam Sandwich Plates," ASME J. Eng. Mater. Technol., **128**(3), pp. 366–374.

[30] Barenblatt, G. I., 1978, *Similarity, Self-Similarity and Intermediate Asymptotics*, Girometeoizdat, Moscow.

[31] Barenblatt, G. I., 1996, *Scaling, Self-Similarity and Intermediate Asymptotics*, Cambridge University Press, Cambridge, UK.

[32] Muki, R., and Westmann, R. A., 1974, "Crack Emanating From an Open Notch," J. Elast., **4**(3), pp. 173–186.

[33] Westmann, R. A., 1975, "Geometrical Effects in Adhesive Joints," Int. J. Eng. Sci., **13**, pp. 369–391.

[34] Hutchinson, J. W., and Suo, Z., 1992, "Mixed Mode Cracking in Layered Materials," Adv. Appl. Mech., **29**, pp. 64–191.

[35] Agrawal, A., and Karlsson, A. M., 2006, "Obtaining Model Mixity for a Bimaterial Interface Crack Using the Virtual Crack Closure Technique," Int. J. Fract., **141**, pp. 75–98.

[36] Toya, M., 1992, "On the Mode I and Mode II Energy Release Rates of an Interface Crack," Int. J. Fract., **56**, pp. 345–352.

[37] Bažant, Z. P., and Xi, Y., 1991, "Statistical Size Effect in Quasi-Brittle Structures: II. Nonlocal Theory," J. Eng. Mech., **117**(11), pp. 2623–2640.

[38] Rice, J. R., 1988, "Elastic Fracture Mechanics Concepts for Interface Cracks," ASME J. Appl. Mech., **55**, pp. 98–103.

[39] Caner, F. C., and Bažant, Z. P., 2009, "Size Effect on Strength of laminate-Foam Sandwich Plates: Finite Element Analysis With Interface Fracture," Composites, Part B, **40**(5), pp. 337–348.

[40] 2006, ABAQUS/Standard Users Manual, *Version 6.6*, Hibbitt, Karlsson & Sorensen Inc., Pawtucket, RI.